Sensitivity of Global Circulation Response to a Southern Ocean Zonal Wind Stress Perturbation

Carlos Cruz[a] and Barry A. Klinger[a,b]

[a]Department of Atmospheric, Oceanic, and Earth Sciences, George Mason University, MS 6A2, 4400 University Drive, Fairfax, VA 22030, USA

[b]Center for Ocean-Land-Atmosphere Studies, 4041 Powder Mill Rd, Suite 302, Calverton, MD, 20705, USA.

Corresponding Author: Barry Klinger, klinger@cola.iges.org, phone: 001-301-902-1271.

Submitted to *Ocean Modelling*, March 2009

Abstract

Previous studies indicate that Southern Ocean wind stress may drive global oceanic overturning variability on decadal timescales. An experiment with a perturbation to a near-global ocean model with realistic topography and forcing (Klinger and Cruz, 2009) raises questions about the evolution of the overturning anomaly. What determines the relative strength of the Atlantic and Pacific response? Is the model's large Indo-Pacific response due to the great width of the Indo-Pacific basin? What is the relationship between the initial response and the final equilibrium? What determines the timescale of the response? These questions are addressed through experiments with a primitive equation model (MOM4) in which the sensitivity of the response to basin width and Atlantic-Pacific density differences are tested.

Pacific overturning anomaly is very roughly proportional to basin width. The North Pacific stratification has little influence on the initial response but strongly affects the final equilibrium response. For strongly stratified North Pacific, the Pacific's transient overturning anomaly is much stronger than its final value, implying a large decadal response.

Response timescales are proportional to the global basin width, consistent with shallow water theory. Mass budgets indicate that cross-isopycnal flow anomalies can be ignored for the first few decades (as in the simplest shallow water models), but become increasingly important afterwards. The response of a single-basin configuration is independent of horizontal resolution, horizontal viscosity, and the use of unequal tracer and momentum timesteps. This strengthens the conclusion that on decadal scales, the behavior is dominated by Rossby wave dynamics and is independent of the detailed behavior of the Kelvin waves.

Keywords: Ocean; Circulation; Modeling; Meridional Overturning

1 Introduction

Klinger and Cruz (2009) use a numerical model with realistic topography and forcing to show how the ocean responds to a sudden increase in the strength of the zonal westerlies over the Southern Ocean. They find that in both the Atlantic and Indo-Pacific basins, the meridional overturning streamfunction Φ evolves over the 80 yr perturbation experiment. In the southern hemisphere, the magnitude of Φ' (the streamfunction anomaly relative to the unperturbed state) in the Indo-Pacific is 2–3 times greater than in the Atlantic during much of the 80 year experiment.

In the steady state, our understanding of the relationship between Southern Ocean wind stress and global overturning is based on the idea that the Ekman upwelling in the Southern Ocean provides part of the source for North Atlantic Deep Water (NADW) downwelling in the northern North Atlantic (Toggweiler and Samuels, 1995). The dense water flowing in the Drake Passage latitude at great depth comes from a dense source in the northern hemisphere. This suggests that an increase in Southern Ocean wind stress should lead to an increase in the Φ in the Atlantic, which has the densest northern hemisphere surface water, rather than in the Indo-Pacific. However, to the authors' knowledge, the direct sensitivity of steady-state Pacific overturning to wind has not been tested with numerical models. Toggweiler *et al.* (2006), De Boer *et al.* (2008) and Rahmstorf and England (1997) looked at coupled atmosphere-ocean experiments (with idealized atmospheric models) which allowed ocean-atmosphere feedback to make significant changes to ocean surface density in response to a Southern Ocean wind perturbation. These experiments did find a significant Pacific overturning sensitivity to Southern Ocean wind stress because of surface density changes driven by the wind perturbation. It is well known that small changes in surface density at multiple high-latitude sites can greatly alter the global overturning patterns (for instance Manabe and Stouffer, 1988; Marotzke and Willebrand, 1991; England, 1993; Hughes and Weaver, 1994; Klinger and Marotzke, 1999; Saenko *et al.*, 2004). Here we are interested in the direct effect of the wind stress when surface density perturbations are suppressed by strong surface restoring conditions. This allows us to isolate distinct mechanisms of influence.

The realistic-basin experiment in Klinger and Cruz (2009) did not run long enough to test our expectation that Φ' evolved to a new equilibrium dominated by overturning in the Atlantic. The large Indo-Pacific transient Φ' does not contradict this expectation, but it raises the question of what determines the relative strength of the Pacific and Atlantic transients.

Another question raised by Klinger and Cruz (2009) concerns the timescale over which the system evolves. What sets it? McDermott (1996), Brix and Gerdes (2003) and Delworth and Zeng (2008) also find a multidecadal timescale in general circulation models driven by switched-on Southern Ocean winds, but do not seek to explain this timescale. Johnson and Marshall (2002, 2004) do a careful analysis of the transient behavior associated with the switch-on of NADW production. Similarly, Cessi and Otheguy (2003) analyze basin modes associated with wind oscillating on decadal periods. Johnson and Marshall (2002) find that the adjustment timescale for overturning is proportional to (but much longer than) the time it takes Rossby waves to zonally traverse the basin. Cessi *et al.*(2004) find lag timescales of decades to a century for pycnocline adjustment to an oscillating change in NADW forcing.

The studies of Johnson and Marshall, Cessi and Otheguy, and Cessi *et al.*are conducted with shallow water models. The advantage of their studies is the relative mathematical simplicity of the linear shallow water equations, but the dynamics are idealized and do not include first-order features such as vertical diffusivity, large lateral variations in stratification, interaction between background circulation and perturbation, and vertical structure in both forcing and response beyond the first baroclinic mode. Despite these differences, Cessi *et al.*(2004) do find quantitatively similar behavior between a shallow water and a general circulation model.

Here we conduct experiments which aim to be a bridge between shallow water theory and realistic general circulation models. Like Klinger and Cruz (2009), we use a general circulation model with realistic dynamics. Like some of the other studies, we use simplified geometry and forcing. Thus we are able to vary parameters systematically, but there is a closer correspondence between these experiments and the real world than shallow water studies can have.

Our simplified geometry consists of a double basin corresponding to the Atlantic and Pacific oceans and connected by a zonally-periodic Southern Ocean. We test the hypothesis that the Φ' is initially stronger in the Pacific than in the Atlantic because of its larger basin width. To do this, we compare pairs of experiments with wide and narrow basin Pacific basin width. Each experiment pair consists of a "base run" integrated to nearly steady state, and a "perturbation run" in which the Southern Ocean wind stress is abruptly increased and the system integrated to a new steady state. The width-sensitivity experiments also allow us to test the shallow water result that the evolution timescale of the system is proportional to the basin width. To filter out interactions between different basins, we conduct single-basin experiments to test sensitivity of the wind-driven perturbation to the basin width.

We also conduct experiments in which the northern North Pacific surface density is varied. Along with geometry, the difference in northern hemisphere surface density is a defining characteristic differentiating "Pacific" and "Atlantic" basins in the real world and in models. Because changing the surface density alters the stratification and hence Rossby wave speed at the Pacific northern boundary, it tests Cessi and Otheguy's idea that the high latitude Rossby wave transit time sets the timescale for the entire basin. Moreover, we find that several aspects of the sensitivity to the wind depends strongly on the North Pacific surface density.

Since it takes thousands of years for the deep meridional overturning circulation to reach equilibrium, we would like to conduct our experiments with somewhat coarse resolution

(2^o) and with the long tracer timesteps of the Bryan (1984) acceleration method. Klinger and Cruz (2009) use HYCOM for the realistic-topography experiment, and find that the Bryan method induces apparently-spurious variability into the system. In our sensitivity experiments here, we use MOM4, which does not have this problem.

Because the Bryan (1984) method distorts the dispersion relation of Kelvin waves and short (compared to the deformation radius) Rossby waves, it is not a good technique to use if the behavior of the system depends on these waves. Similarly, the relatively high viscosity demanded by coarse resolution and the resolution itself can distort Kelvin wave propagation, particularly in a B-grid model such as MOM (Hsieh *et al.*, 1983). Therefore, we conduct single-basin experiments which test the sensitivity of the results to the resolution and to the use of the acceleration method. Showing that the results are not sensitive to these features enhances our confidence in our model results. Because the largest changes in basin-scale overturning occur on decadal scales, we believe that the evolution is governed by long Rossby waves, rather than Kelvin waves or short Rossby waves or advection by western boundary currents (which are also sensitive to resolution and friction). Thus the resolution and timestep experiments will be additional tests that our dynamical ideas are correct.

2 Model Description and Configuration

2.1 Geometry and Forcing

Our experiments are conducted using the Geophysical Fluid Dynamics Modular Ocean Model version 4 (MOM4; see Griffies, *et al.*, 2004), a primitive equation level model with B-grid discretization. We run most experiments at the same $2^o \times 2^o$ horizontal resolution except for one experiment run at $1^o \times 1^o$ horizontal resolution. All basins have a constant basin depth of $H = 4000$ m and 20 vertical levels with level thickness ranging from 30.5 m at the top to 369.5 m at the bottom. Two geometries are considered: a single basin with a reentrant channel that models the circumpolar connection in the southern ocean latitudes (Table 1) and a double-basin geometry with a similar reentrant channel (Table 2). All the basins are sectors which extend from 63^{o}N to 68^{o}S and have zonal width Λ (in degrees longitude) which varies between basins and experiments. For the single basin experiments, representing an Atlantic basin, we consider two configurations: $\Lambda = 40^o$ and $\Lambda = 80^o$. The double basin experiments (Fig. 1) represent an Atlantic (40^o wide) and a Pacific basin. The Pacific basin is 40^o in "narrow Pacific" experiments and 120^o in "wide Pacific" experiments. The Atlantic basin and even the wide Pacific basin are somewhat narrower than the real ocean basins in order to minimimize computational expense.

The circumpolar connection is modeled by a periodic channel extending from 54^{o}S to 62^{o}S and having a depth of 1526 m. The meridional ridge with a zonal extent of size 10^o is arranged to block the deep part of the Drake passage latitude. The minimum depth is somewhat less than is commonly used in models (Toggweiler and Samuels, 1995; McDermott, 1996; Gnanadesikan, 1999), but reflects the relatively shallow depths of the Kerguelen rise of the Indian Ocean and of the channels between the South Sandwich Island of the South Atlantic.

At the surface, temperature and salinity in each basin are restored to time-independent, zonally uniform mean values with a restoring time constant of 30 days. Profiles are broadly based on climatological values for the real ocean, with the North Atlantic restored to saltier and hence denser conditions than the North Pacific (Fig. 2a,b) in order to produce an analogue of NADW. Different salinity profiles (Fig. 2a) are chosen in order to vary the target σ_θ difference $\Delta\rho_{*N}$ between the northern boundary of the Atlantic and the Pacific (Fig. 2b). For dense Pacific forcing, $\Delta\rho_{*N} = .299$ kg/m^3, and for light Pacific forcing, $\Delta\rho_{*N} =$ 1.047 kg/m^3. Both wide Pacific and narrow Pacific experiments are forced with dense and light Pacific forcing. Additional wide Pacific experiments are forced with intermediate Pacific density (Pacific salinity given by average of light and dense Pacific cases) and no-mixed-layer forcing (uniform equatorial values of temperature and salinity for North Pacific). Table 2 summarizes the double-basin perturbation experiments. The single-basin experiments are forced with Atlantic-basin temperature and salinity only.

The base runs are driven by zonally-uniform zonal wind stress $\tau(\phi)$ (where ϕ is latitude) which is broadly based on observed climatology (Fig. 2). In the perturbation experiments, we add a Gaussian shaped function $\tau'(\phi)$ in the westerly wind stress region (south of 30^o S) which reaches a maximum just north of the zonally periodic region of the Southern Ocean (Fig. 2c). Each perturbation run begins at the end of a corresponding base run. All anomaly variables, such as Φ', are defined by subtracting their value at $t = 0$, which is defined as the beginning of the perturbation run.

In the wide single-basin experiment, the maximum strength of the perturbation is equal to the base run maximum southern hemisphere westerlies. In the narrow single-basin experiment, the perturbation is twice the amplitude. Therefore the northward Ekman volume transport perturbation, which is proportional to basin width and τ', is the same in the two experiments. In all double basin experiments, τ' is the same as in the wide single-basin experiment. In the double basin experiments, it is not helpful to vary τ' based on basin width because the relative widths of Atlantic, Pacific, and total domain in the wide Pacific and narrow Pacific experiments are all different.

2.2 Mixing Parameters and Base Run Equilibrium

The vertical diffusivities of temperature and salinity are uniform throughout the domain and set to $\kappa_V = .5 \times 10^{-4}$ m^2/s. Horizontal viscosity is also uniform, with $\nu_H = 2.5 \times 10^5$ m^2/s. Density and thickness are diffused laterally along isopycnals with κ_I=1000 m^2/s. Except as noted below, all runs are conducted using the Bryan (1984) acceleration method, with a momentum timestep of 1 hr and a tracer timestep of 12 hr. The long-term evolution of the system is governed by the density field, so the tracer timestep (rather than momentum timestep) defines time elapsed since beginning of each integration.

Here and in the rest of the paper, overturning Φ and overturning anomaly Φ' refers to the sum of the meridional streamfunctions associated with explicit model velocities and "bolus velocities" associated with the Gent-McWilliams eddy parameterization (Gent and McWilliams, 1990; Gent *et al.*, 1995). These streamfunctions are constructed by zonally integrating the meridional velocity (including meridional bolus velocity) along a constant depth. In subsequent sections, Φ'_M will denote the net volume transport anomaly as measured by the maximum Φ' at each latitude and time.

Base runs are integrated until $|d\Phi(\phi, z)/dt|$ is decreasing and $|d\Phi(\phi, z)/dt \leq .02$ Sv/century (z is depth, Sv $= 10^6$ m^3/s). Generally the base runs are integrated for 2000 yr. For narrow-dense and wide-dense experiments, the initial condition consists of horizontally uniform temperature and salinity. Initial conditions for other experiments are the final state of previous runs

In equilibrium, Pacific Φ and northern Pacific stratification are sensitive to Pacific surface density. As has been discussed in previous papers (Marotzke and Willebrand, 1991; Hughes and Weaver, 1994), the relative surface density of North Pacific and North Atlantic determine which basin produces deep mixed layers and the sinking limb of the overturning cells. Small changes in this density difference can produce big changes in the overturning (Klinger and Marotzke, 1999). Our experiments follow this pattern, with both mixed layer and sinking near the northern boundary of the Pacific getting shallower as the surface is made lighter in different experiments (Fig. 3a-c). The Atlantic overturning and stratification (Fig. 3d) is less sensitive to the Pacific variations. The narrow Pacific runs (not shown) show similar behavior to the wide Pacific runs. It is important to remember that the model surface density differs somewhat from the restoring values, due to ocean heat and freshwater transport. The narrow Pacific experiments have somewhat different surface densities than corresponding wide Pacific experiments. As Sec. 4 shows, these small differences have observable consequences for the perturbation behavior.

2.3 Sensitivity to Bryan (1984) Acceleration and Resolution

The single-basin configuration is used to test the sensitivity of the results to tracer timestep and to horizontal resolution and horizontal viscosity. The narrow-basin perturbation experiment is repeated with a tracer timestep equal to the momentum timestep of 1 hr instead of 12 hr used for the other experiments. To insure that there are no other changes due to switching the timestep, the base run is continued for 20 yr with the short timestep before applying the wind perturbation. There is a change of .15 Sv in peak overturning due to the change in timestep. By the end of the 20 yr integration, the rate of change of the overturning reduces to .0002 Sv/year, indicating that the system is close to equilibrium. The perturbation experiment is run for 30 yr.

A somewhat different pair of experiments is conducted to explore the effect of horizontal resolution. To avoid having to run a long integration at high resolution for the base run to reach equilibrium, the comparison between high resolution and low resolution experiments is done as a perturbation from rest. The low resolution experiment has the same geometry as the other single-basin experiments. High resolution experiments have the same geometry interpolated to a 1^o latitude-longitude grid. The initial condition has uniform salinity ($S = 34.0$ psu) and has horizontally-uniform potential temperature $T = \Delta T e^{z/D}$, where $\Delta T = 22$ C, $D = 750$ m, and $z < 0$ is the height relative to sea-level. The windstress in the perturbation-from-rest experiments is equal to the windstress perturbation in the other single-basin experiments (that is, the perturbation run windstress minus the base run windstress). There is no surface flux of heat or freshwater.

The higher resolution allows for a smaller viscosity. One 1^o resolution experiment is conducted with the same viscosity as the 2^o experiments ($\nu_H = 250 \times 10^3$ m^2/s) and another is conducted with $\nu_H = 10 \times 10^3$ m^2/s. The perturbation from rest experiments are conducted for 20 yr. Table 1 summarizes all the single-basin perturbation experiments.

3 Single Basin Results

3.1 Numerical Sensitivity Experiments

The numerical sensitivity experiments show that both the Bryan (1984) unequal timestep technique and coarse resolution have little effect on the overturning anomaly driven by a Southern Ocean wind perturbation.

Comparing the unequal timestep experiment to the narrow single basin experiment, we see that the spatial structure and magnitude of the overturning anomaly is nearly identical in the two runs at about 26 yr (Fig. 4a) as well as at other times (not shown). The time evolution of Φ' is also identical, as measured by Φ'_M (Fig. 4b). Note that in these experiments, the overturning anomaly is the same as the overturning, since the "base run" is simply the resting initial condition.

The Southern Ocean wind perturbation on a resting ocean produces a response that grows at first and then decays in time (McDermott, 1996). The time evolution of Φ'_M in the perturbation from rest experiments are fairly insensitive to resolution and horizontal viscosity (Fig. 5a). The low ν_H run has slightly larger amplitude, but the evolution of Φ'_M at specific latitudes (Fig. 5b,c) shows similar timescales to the 2^o run. At each latitude, it reaches the maximum value at the same time. When scaling Φ'_M at each latitude by its maximum value at that latitude, the scaled Φ'_M is close to the 2^o experiment, indicating a similar decay rate.

3.2 Width Sensitivity Experiments

In simplified, reduced-gravity configuration, the timescale of the response of the system to a perturbation in the overturning is proportional to the basin area, and hence to its width (Johnson and Marshall, 2002). We test the sensitivity to width in our more complex configuration by conducting an additional unequal-timestep experiment with double the basin width (80^o).

The qualitative behaviors of the narrow and wide basins are very similar to each other. The final Φ' looks like the transient shown in Fig. 4a, with Φ'_M in the two runs within about 10% of each other. These volume transport anomalies overshoot their final values by a small amount. In the narrow basin experiment, such overshoots are less than 10% larger than the final values. In the wide basin experiment, the overshoots are less than 25% bigger than their final value except for larger values north of 40^o N.

In order to compare the timescales of the two experiments, we normalize the volume transport anomaly by its final value at each latitude,

$$\Phi'_N = \Phi'_M(t, \phi)/\Phi'_M(t_{\text{final}}, \phi). \tag{1}$$

It is also useful to define a width-adjusted time,

$$t_W = t\Lambda/\Lambda_W, \tag{2}$$

where Λ_W is the width of the wide basin. Superimposing contour plots of $\Phi'_N(t_W, \phi)$ from the two runs (Fig. 6), we see that over a wide range of latitudes, both experiments take about the same width-adjusted time to reach 50%, 75%, and 90% of their final value. This indicates that the characteristic timescale for the basin is proportional to width, as in Johnson and Marshall (2002). Johnson and Marshall and Klinger and Cruz (2009) also find a big difference between the faster timescale of the forcing hemisphere and the slower timescale of the other hemisphere. In the experiments with MOM4, we don't find such a strong distinction. The timescale increases linearly with latitude from 30^o S to 30^o N.

McDermott (1996) did not publish as detailed a description of the time evolution of his single-basin experiment, but overturning at 60^o N (northern boundary is at 72^o N) decays with an e-folding scale of about 90 yr (see McDermott, 1996, Fig. 18). Our wide-basin run has an e-folding scale of about 30 yr at an equivalent latitude (53^o N, northern boundary at

64^o N). It is not clear why the timescale is so different for such similar experiments. In our experiments, there tends to be especially large variations between runs near the northern boundary, and it is not clear that McDermott's figure is representative of the basin as a whole.

4 Double Basin Results

While the main focus of this paper is on the transient, rather than equilibrium, response to a wind perturbation, it is useful to start with the final equilibrium. Knowing the steady state that the system is tending towards will help us characterize the system's evolution towards that steady state.

4.1 Final Equilibrium Overturning Anomalies

Overturning anomaly Φ' in the Atlantic basin (Fig. 7a) looks similar to the transient and final values in the single-basin case (McDermott, 1996 [Fig. 18c]; see Sec 3 above). A single overturning cell (Fig. 7) fills nearly the entire basin north of the zonally periodic channel. This cell, which augments the NADW cell of the base run (Fig. 3a), is qualitatively similar for all the double basin experiments.

In the perturbation runs, the sinking region in the North Atlantic extends further southward from the northern boundary region than it does in the base runs. This is manifested in Φ' as a narrow, southern-sinking cell confined to the northern boundary. Such a cell does not appear in the single-basin experiments, though a similar cell is seen at 20 yr (subsequently disappearing) in a realistic-topography experiment (Fig. 15 of Brix and Gerdes, 2003).

The northern-sinking overturning anomaly in the Pacific shows considerable sensitivity to north Pacific surface density (Fig. 7b-d). Generally speaking, the lighter and more stratified the northern boundary (Fig. 3b-d), the shallower and weaker the anomaly cell. The northward extension of the anomaly cell also decreases for lighter northern surface water.

The trend with density is consistent with the single-basin experiments of McDermott (1996) and Sec. 3. For an Atlantic-like basin with an unstratified northern boundary (where deep water formation occurs), the wind stress generates a strong northern-sinking anomaly that persists indefinitely. When the initial state is a resting, uniformly-stratified basin, by 50 yr Φ' has weakened considerably from larger values in the first decade. In our dense Pacific case the Pacific stratification looks much like the Atlantic and so responds with a strong, deep Φ' like the Atlantic, while in the light Pacific and (even more so) the no-mixed layer case the Pacific looks more like an unstratified fluid which does not support a steady, basin-filling overturning. This is also consistent with Toggweiler's original explanation: to the extent that the Ekman transport in the Southern Ocean can connect to deep (or intermediate) water formation in the north, that Ekman transport can drive a remote overturning.

To compare the magnitude of volume transport anomaly in different basins of different widths, we scale Φ'_M by the zonally integrated Ekman transport $\Delta\Phi$ in that basin ($\Delta\Phi_P$ for Pacific, $\Delta\Phi_A$ for Atlantic, and $\Delta\Phi_G$ for the global domain). These Ekman transports are calculated at 51^o S, which is the northern edge of the zonally periodic channel and hence considered the most relevant for driving the large-scale overturning (Toggweiler and Samuels, 1995; Gnanadesikan, 1999).

The Pacific Φ'_M (Fig. 8a) shows the great sensitivity to northern Pacific density seen in Fig. 7. The dense Pacific experiment has about 5 times as large a Φ'_M as the no-mixed-layer experiment in the vicinity of the equator—greater near the northern boundary. In the Atlantic (Fig. 8b), Φ'_M also depends on Pacific density. The larger Pacific Φ'_M is, the smaller is Atlantic Φ'_M. This would be expected if the total overturning anomaly driven by Southern Ocean winds are a fixed fraction of $\Delta\Phi_G$, with the relative density of northern Pacific and northern Atlantic merely controlling the proportion of the global Φ'_M that flows into each basin.

In fact, global Φ'_M increases with northern Pacific density (Fig. 8c), though the range over all the experiments is about a factor of 2 rather than the factor of 5 displayed by the Pacific. Here Φ'_M is defined as the maximum (in depth) of the sum of the Atlantic and Pacific streamfunction anomalies; simply adding Φ'_M from the individual basins gives a similar result. As Gnanadesikan (1999) and Klinger *et al.* (2003, 2004) discussed, we can think of the Ekman transport anomaly $\Delta\Phi_G$ at the northern edge of the channel region "feeding" a local eddy-compensated response directly under the Ekman pumping, and a global cell with remote sinking in the northern hemisphere. Changing the Pacific width evidently changes the balance between these two pathways. The single basin experiments (circles in Fig. 8c) have a similar normalized Φ'_M, indicating that the influence of the wind on the net overturning is relatively insensitive to the number of basins.

It is not trivial to compare the surface density in the model to those in the real world. Some complicating factors not present in the model include the seasonal cycle and the complicated geometries of marginal seas and sills in the vicinity of the deep water formation sites in the real world. We use the World Ocean Atlas 2001 1/4 degree fields (www.nodc.noaa.gov/OC5/indprod.html) subsampled to a 1/2 degree grid. If we simply compare maximum surface annual-mean densities in the North Atlantic (south of Iceland) and the North Pacific, we find that the Pacific maximum is about 1.2 kg/m^3 lighter than the Atlantic, which in turn is about 6 kg/m^3 denser than typical equatorial values. The numerical experiment which corresponds most closely to this range is the wide light-Pacific experiment, with a northern Pacific-Atlantic density difference of 1.0 kg/m^3.

Pacific Φ'_M increases with basin width, as we hypothesized. For light Pacific experiments, $\Phi'_M/\Delta\Phi_P$ is the same for wide Pacific and narrow Pacific, so that Φ'_M is proportional to width (Fig. 8a). The same figure shows that for the dense Pacific experiments, $\Phi'_M/\Delta\Phi_P$ is significantly larger for the wide Pacific than for the narrow Pacific. The narrow Pacific Φ' is also confined to shallower depths. However, these are indirect effects of density. Rather than using the target surface restoring values to measure density, we can measure $\Delta\rho_{NB}$, the vertical range of the zonal averaged density at the northern boundary of the Pacific. Because $\Delta\rho_{NB}$ is affected by the flow, which is affected in turn by the width of the Pacific, the wide-dense Pacific run has a smaller $\Delta\rho_{NB}$ than the narrow-dense Pacific. $\Phi'_M/\Delta\Phi_P$ depends cleanly on $\Delta\rho_{NB}$ (Fig. 9), implying that Φ'_M is proportional to width if we control for actual north Pacific density.

The Atlantic Φ'_M also increases when Pacific basin width increases (Fig. 8b), especially in the light Pacific experiments. This indicates that some of the Ekman transport perturbation in the Pacific sector drives a geostrophic flow into the Atlantic in the steady state.

4.2 Transient Overturning Anomalies

In the first decade of the perturbation, Φ'_M in each basin and for the global domain is not sensitive to north Pacific density (Fig. 10). This is in sharp contrast to the final steady state (previous subsection). The vertical structure (not shown) is also similar in all the runs, with the overturning anomaly cell filling the entire water column. The volume transport anomaly in each basin is proportional to the Ekman transport in that basin (Fig. 10), as in the final steady state, with a similar proportionality constant for all three basins. Thus the overturning response in the Pacific (Fig. 10a) is larger than in the Atlantic (Fig. 10b) for the wide-Pacific cases.

Differences in Φ'_M between runs with different Pacific densities appear after the first decade (Fig. 11). Pacific volume transport (Fig. 11, left panels) near the northern boundary increases monotonically in time in most of the experiments. In the south (just to the north of the wind perturbation), Φ'_M increases to a maximum value and then decreases after a few decades. The relative prominence of these two regions varies with Pacific density. In the dense-Pacific case, the regime of monotonic increase covers nearly the entire Pacific (Fig. 11a). For decreasing north Pacific density (Fig. 11b,c), the regime with increase-followed-by-decrease expands until it fills the entire basin in the no-mixed-layer case (not shown, but similar to Fig. 11c except for decreasing Φ'_M after about 30 yr north of 30^o N. The narrow-Pacific experiments have qualitatively similar $\Phi'_M(\phi, t)$ to the wide-Pacific runs.

We can think of the temporal behavior of the Pacific Φ'_M as a stitching together of the initial behavior and the final behavior. Initially the Pacific volume transport anomaly grows regardless of northern Pacific density. In the end, Φ'_M is quite sensitive to this density. If the final Φ'_M is weak enough, Φ'_M must decrease from its earlier values in order to reach this final state. The weaker the final Φ'_M, the more dramatic and widespread the decrease.

The Atlantic volume transport (Fig. 11e) increases monotonically over almost the entire domain for all the runs except the narrow-dense experiment, in which it decreases substantially after about 100 yr throughout most of the domain. The reason for this exception is not clear. The global Φ'_M looks similar to the Pacific (Fig. 11d,f), even in the narrow-basin cases for which Pacific Φ'_M is not much larger than Atlantic Φ'_M.

Characterizing the time evolution of Φ'_M is made difficult by the qualitative differences between different experiments (for instance, Fig. 11, left panels). The South Pacific Φ'_M reaches its maximum value at a similar time in all the wide-Pacific experiments (including the no-mixed-layer experiment, not shown). The maximum occurs at around 10–20 yr, with a lag of up to around 10 yr from 30^o S to the northernmost latitude at which the maximum occurs. The timescale for decay from the maximum value increases dramatically as the northern Pacific density decreases (Fig. 11, left panels): a few decades for the wide dense run compared with over 1000 yr for the wide-light. The time it takes the monotonically-increasing region (in the north of the Pacific) to get close to its final value has the opposite dependence on density: wide-dense takes a few hundred years while wide-light takes a few decades.

In the Atlantic, we use Φ'_N (Φ'_M normalized by its final values) to measure the evolution timescales, as we did for the single-basin experiments in Section 3 above. The timescales are quite sensitive to north Pacific density. Over most of the domain north of 30^o S, the timescale is longer for more stratified North Pacific. To reach $\Phi'_N = .5$, all the runs took less than 10 yr in the southern hemisphere and from 12 yr (dense Pacific) to 51 yr (light Pacific) to 124 yr (no-mixed-layer) at 30^o N. Φ'_N at 30^o N took from 100 yr (light Pacific) to about 600 yr (light and no-mixed-layer) to reach .75. Thus in the Atlantic, there is not a clean distinction between the decadal-scale response and a centennial-scale response.

Cessi and Otheguy (2003) suggest that the basin-wide response to a wind perturbation acts like a mode with a timescale set by the time it takes long Rossby waves to cross the basin at the high latitude boundary. The Rossby wave speed is proportional to the gravity wave speed and hence to $\sqrt{\Delta\rho_{NB}}$, so that the denser the surface water of the North Pacific, the longer the transit speed. Our experiments show mixed evidence for this assertion: as Rossby wave transit time at the northern boundary of the Pacific increases, the timescale increases for the North Pacific, stays the same for the South Pacific, and decreases for the Atlantic.

The evolution timescales depend on basin width in a somewhat simpler way. Based on Φ'_N, the timescales for both the Atlantic and Pacific are a factor of 2 longer in the light wide-Pacific experiment than in the light narrow-Pacific experiment (Fig. 12). One could argue that this is consistent with shallow water theory (Johnson and Marshall, 2002; Cessi and Otheguy, 2003), since the entire domain in the wide-Pacific experiments is double the width of the narrow-Pacific experiments. It is interesting that the timescales of the individual basins scale the same as the entire domain, even though the Pacific width is tripled in the wide-Pacific case and the Atlantic width is unchanged. This indicates that even on decadal scales, the dynamics of the two basins are coupled to each other.

Finally, though Φ'_M in the forcing region (south of 30^o S) is very close to its final value within the first year or so, other changes occur there over time. For instance, we examined the vertical structure of the global Φ' in the wide-light experiment. Φ' undergoes strong changes over the first few decades and significant changes over the following centuries.

Initially, the northward Ekman perturbation is balanced by a return flow that is distributed somewhat evenly throughout the water column. This return flow becomes more concentrated in narrower depth ranges in the top kilometer and the bottom kilometer of the water column at high southern latitudes.

4.3 Cross Isopycnal Flow

For a steady-state system, conservation of mass implies that any region in which there is a net inflow or outflow between two isopycnal surfaces must have water flowing through an isopycnal surface and hence changing its density. For this reason, diabatic processes such as subsurface mixing help determine the flow (see for instance Bryan, 1987, and Gnanadesikan, 1999). Scaling analyses based on this idea indicate that for realistic magnitudes of diapycnal mixing, the associated time-scale to come to equilibrium is several—or perhaps many—centuries. Over times that are very short compared to this multicentennial timescale, the density stratification should not have been able to change enough to make a large change in diapycnal mixing, so the the initial evolution should be governed by wave dynamics. One is therefore tempted to neglect the cross-isopycnal flow. In this adiabatic limit, a net inflow or outflow between two isopycnals increases the volume of water between the isopycnals, thus moving the isopycnals vertically. Such an assumption is used by Johnson and Marshall (2002) and Cessi and Otheguy (2003).

Here we diagnose the strength of the cross-isopycnal flow anomaly in our numerical model. We analyze Pacific and Atlantic basins from the wide light Pacific experiment. We compare two vertical velocities. The first vertical velocity is based on the total streamfunction anomaly between latitudes ϕ_1 and ϕ_2:

$$w(z,t) = (\Phi'(\phi_2, z, t) - \Phi'(\phi_1, z, t))/A \tag{3}$$

where A is the area of the basin between the two latitudes. For the other velocity, we select a given isopycnal σ and calculate the rate of change of its depth $Z(\sigma, \phi, \lambda, t)$ between successive times $t_1 = t - .5\delta t$ and $t_2 = t + .5\delta t$:

$$w_I(\sigma, t) = \frac{1}{A\delta t}\int (Z(\sigma, \phi, \lambda, t_2) - Z(\sigma, \phi, \lambda, t_1))dA. \tag{4}$$

We choose $\phi_1 = -30^o$, $\phi_2 = 51^o$ and $Z \approx 1000$ m, a region in which the isopycnals are relatively flat (Fig. 3a,d).

For both the Atlantic and Pacific, the Eulerian area-average vertical velocity w is very close to the area-average isopycnal vertical velocity w_I for the first forty years or so of the perturbation experiment (Fig. 13). For entire first century of the experiment, the two curves are within about 30% of each other. During this period, the downward velocity over most of the basin is associated with the downward motion of the isopycnal. After that, w and w_I diverge significantly. In the Pacific, the density structure approaches a new, steady equilibrium ($w_I \to 0$) while a downwelling anomaly persists over a broad area as in Fig. 7d. In the Atlantic, the $w_I \to 0$ as well, but the new equilibrium has a mean upwelling which partly compensates the much larger downwelling that occurs north of 51^o N (outside the averaging area) as in Fig. 7a. Calculations over smaller latitude ranges within 30^o S to 51^o N show a similar relationship between w and w_I: the two measures of velocity are similar for the first few decades and then by about 100 yr.

5 Summary and Conclusions

We studied the global overturning circulation's response to Southern Ocean wind stress perturbation through a series of experiments with idealized geometry and forcing but with dynamics as realistic as a non-eddy-resolving general circulation model can allow.

The experiments were motivated by the realistic-geometry experiment of Klinger and Cruz (2009) in which switched-on Southern Ocean winds drove a stronger overturning response in the Indo-Pacific than in the Atlantic. We hypothesized that initially, the response is stronger in the Indo-Pacific because the Indo-Pacific width is greater than the Atlantic width. We further hypothesized that such sensitivity to the Ekman transport in a given sector of the ocean would disappear as the system approached a new steady state. In the final steady state, we expected the overturning anomaly to shift to the Atlantic, contributing to North Atlantic Deep Water (NADW) formation, as in Toggweiler and Samuels (1995).

Our idealized experiments show that in both the initial decadal-scale behavior and the final equilibrium, the Pacific overturning anomaly is proportional to Pacific basin width. Thus the initial large Pacific sensitivity to Southern Ocean wind stress is a product of the Pacific width, as we hypothesized. The final behavior is more complicated, and depends critically on the relative density of the northern North Atlantic (the densest northern hemisphere water) and the northern North Pacific. As the Pacific density approaches Atlantic values, the North Pacific looks more like the North Atlantic both in the background stratification and in the strength of the response. As the Pacific density is decreased, the Pacific becomes more stratified and less able to support a wind-driven overturning anomaly in the steady state. There are undoubtedly other subtleties in the equilibrium response of the two basins (see for instance Gnanadesikan *et al.*, 2007; Hirabara *et al.* 2007). The real ocean may be most like the wide light-Pacific experiment, which has an equilibrium Pacific anomaly concentrated in the top half of the water column with a similar magnitude to the Atlantic.

In the first decade after imposing the perturbation, the behavior of the system is insensitive to North Pacific density. The transient overturning anomaly in the Pacific tends to reach a maximum in the southern hemisphere after several decades before declining to its final value. The intensity and extent of the maximum overturning depends on the north Pacific density. The transient overturning anomaly in the Pacific increases monotonically to its final value in most of the experiments. Like the simulation in Klinger and Cruz (2009), the southern hemisphere responds more quickly than the northern hemisphere to the wind perturbation, though the distinction between the hemispheres is not as distinct as in Klinger and Cruz (2009) or in the study of Johnson and Marshall (2002). In both single-basin and double-basin experiments, the timescale of the entire system is roughly proportional to the width of the entire basin. This indicates that even during the transient period, both basins are dynamically linked, with the Atlantic response influenced by the width of the Pacific basin.

Some other results give further insight into the dynamics of the response to the wind perturbation. Our numerical sensitivity experiments show that resolution, viscosity, and Kelvin wave speed have a negligible effect on behavior. During the first half century or so of the perturbation experiment, over most of the domain, the downward velocity associated with the overturning anomaly is about the same as the downward motion of the isopycnals. Thus the cross-isopycnal flow associated with the anomaly field is negligible except at very high latitudes. These numerical results all suggest the applicability of Rossby wave dynamics such as in the shallow water studies of Johnson and Marshall (2002, 2004) and Cessi and Otheguy (2003). In those studies, Kelvin waves merely serve to equilibrate the eastern boundary pycnocline, so their speed is irrelevant as long as it is much faster than the Rossby wave speed. Those studies also ignore cross-isopycnal flow except (in the Johnson and Marshall papers) at high latitudes.

Other factors make it harder to directly compare to simple wave models. After the first century, the changing advective-diffusive balance due to the wind perturbation becomes of first order importance. Changes in the vertical structure of the Pacific overturning perturbation over time suggests that higher vertical modes are relevant. Strictly speaking, the concept of vertical modes does not apply to basins in which the vertical structure changes significantly across the basin, as it does in our experiments between the high and low latitudes and between the individual basins. It is still not clear to what extent the detailed behavior of the system is due to wave dynamics in such a meridionally-varying stratification, and to what extent the background flow affects the evolution of the perturbation.

Acknowledgements

The authors were supported by NSF grant OCE-0241916. Two anonymous reviewers gave helpful suggestions.

References

Brix, H., and R. Gerdes, 2003: North Atlantic Deep Water and Antarctic Bottom Water: Their interaction and influence on the variability of the global ocean circulation, *J. Geophys. Res.*, **108**, doi:10.1029/2002JC001335.

Bryan, K., 1984: Accelerating the convergence to equilibrium of ocean-climate models, *J. Phys. Oceanogr.*, **14**, 666–673.

Cessi, P. and P. Otheguy, 2003: Oceanic teleconnections: remote response to decadal wind forcing, *J. Phys. Oceanogr.*, 33, 1604–1617.

Cessi, P., K. Bryan, and R. Zhang, 2004: Global seiching of thermocline waters between the Atlantic and the Indian-Pacific ocean basins, *Geophys. Res. Lett.*, 31, L04302, doi:10.1029/2003GLO19091

Delworth, T. L., and F. Zeng, 2008: Simulated impact of altered Southern Hemisphere winds on the Atlantic meridional overturning circulation, *Geophys. Res. Lett.*, 35, L20708, doi:10.1029/2008GL035166.

de Boer, A. M., J. R. Toggweiler, and D. M. Sigman, 2008: Atlantic dominance of the meridional overturning circulation, *J. Phys. Oceanogr.*, 38, 435–450.

England, M. H., 1993: Representing the global-scale water masses in ocean general circulation models. *J. Phys. Oceanogr.*23, 1523–1552.

Gent, P., and McWilliams, J., 1989: Isopycnal Mixing in Ocean Circulation Models. *J. Phys. Oceanogr.*, 20, 150–155

Gent, P. R., J. Willebrand, T. J. McDougall, J. C. McWilliams, 1995: Parameterizing eddy-induced tracer transports in ocean circulation models, *J. Phys. Oceanogr.*, 25, 463–474.

Gnanadesikan, A, 1999: A simple predictive model for the structure of the oceanic pycnocline, *Science*, **283**, 2077–2079.

Gnanadesikan, A., A. M. de Boer, and b. K. Mignone, 2007: A simple theory of the pycnocline and overturning revisited, in *Ocean Circulation, Mechanisms and Impacts*, Geophysical Monograph Series 173, American Geophysical Union.

Griffies, S. M., M. J. Harrison, R. C. Pacanowski, and A. Rosati, 2004: *A Technical Guide to MOM4, GFDL Ocean Group Technical Report No. 5*, NOAA/Geophysical Fluid Dynamics Laboratory, available online at www.gfdl.noaa.gov.

Hirabara, M., H. Ishizaki, and I. Ishikawa, 2007: Effects of the westerly wind stress over the Southern Ocean on the meridional overturning, *J. Phys. Oceanogr.*, 37, 2114–2132.

Hsieh, W., Davey, M., and Wajsowocz, R., 1983: The free Kelvin wave in finite-difference numerical models, *J. Phys. Oceanogr.*, 13, 1383–1397.

Hughes, T.M.C., and Weaver, A.J., 1994: Multiple Equilibria of an Asymmetric Two-Basin Ocean Model. *J. Phys. Oceanogr.*, 24, 619–637.

Johnson, H. L., and D. P. Marshall, 2002: A theory for the surface Atlantic response to thermohaline variability, *J. Phys. Oceanogr.*, **32**, 1121–1132.

Johnson, H. L., and D. P. Marshall, 2004: Global teleconnections of meridional overturning circulation anomalies, *J. Phys. Oceanogr.*, **34**, 1702-1722.

Klinger, B.A., and Marotzke, J., 1999: Behavior of double-hemisphere thermohaline flows in a single basin. *J. Phys. Oceanogr.*, **29**, 382–399.

Klinger, B. A., and C. Cruz, C., 2009: Decadal response of global circulation to Southern Ocean zonal wind stress perturbation, *J. Phys. Oceanogr.*, in press.

Manabe, S.,and Stouffer, R., 1988: Two Stable Equilibria of a Coupled Ocean-Atmosphere Model. J. Clim., 1, 841–866.

Marotzke, J., and J. Willebrand, 1991: Multiple equilibria of the global thermohaline circulation. *J. Phys. Oceanogr.*, **21**, 1372–1385.

McDermott, D. A., 1996: The regulation of northern overturning by southern hemisphere winds, *J. Phys. Oceanogr.*, **26**, 1234–1255.

Rahmstorf, S., and M. H. England, 1997: On the influence of Southern Hemisphere winds on North Atlantic Deep Water flow, *J. Phys. Oceanogr.*, 27, 2040–2054.

Saenko, O. A., A. Schmittner, and A. J. Weaver, 2004: The Atlantic-Pacific seesaw, *J. Climate*, 17, 2033–2038.

Toggweiler, J. R., and B. Samuels, 1995: Effect of Drake Passage on the global thermohaline circulation, *Deep-Sea Res.*, **42**, 477–500.

Toggweiler, J. R., J. L. Russell, and S. R. Carson, 2006: Midlatitude westerlies, atmospheric CO2, and climate change during the ice ages, *Paleoceanography*, 21, doi:10.1029/2005PA001154.

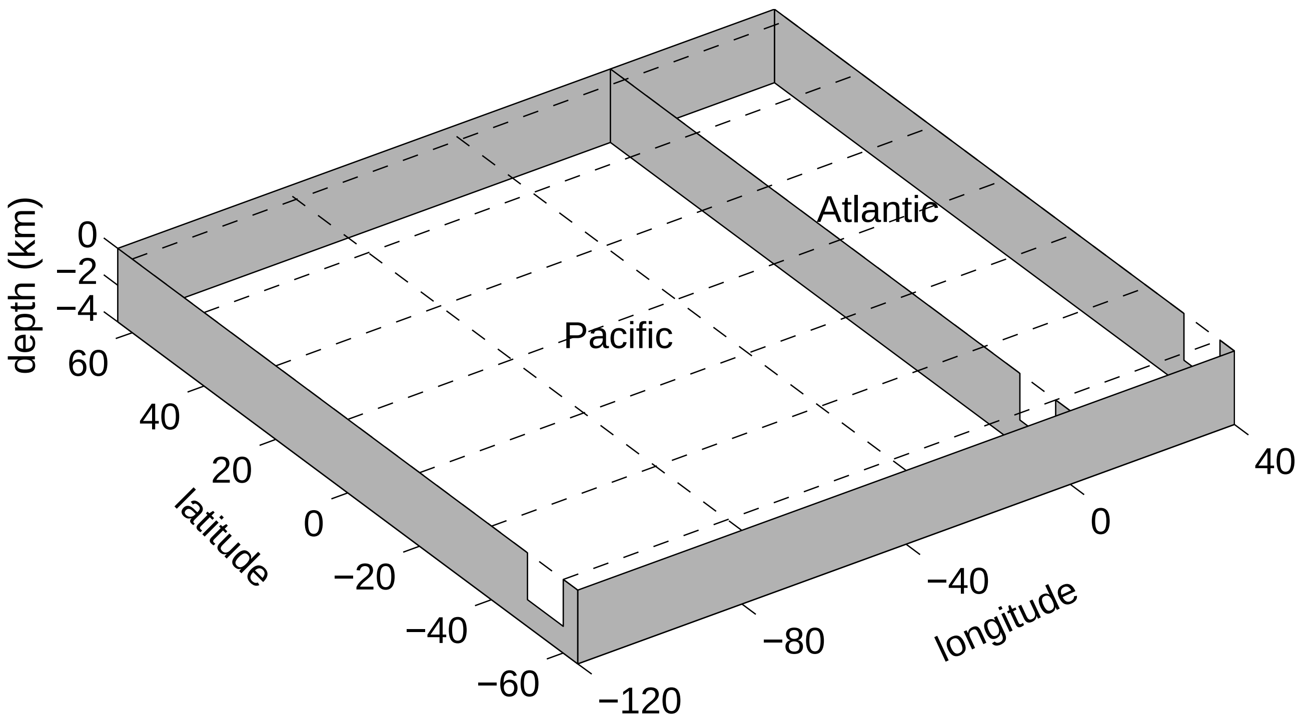

Figure 1: Perspective view of basin geometry for double-basin, wide-Pacific, configuration.

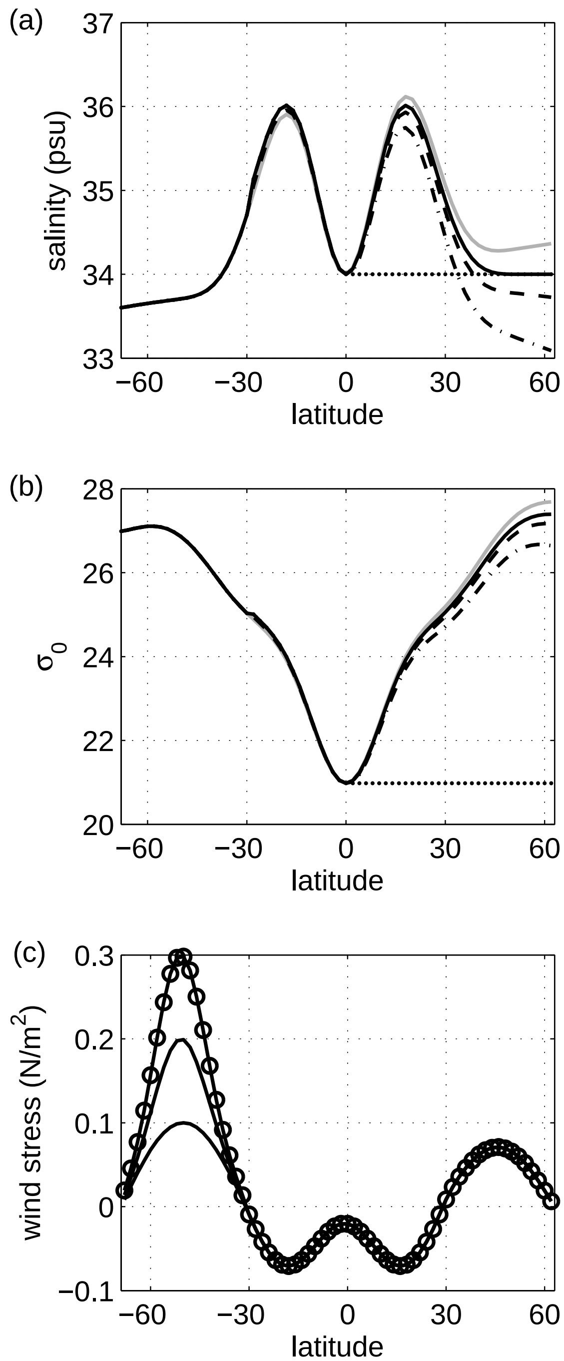

Figure 2: (a) Salinity restoring for Pacific basin (black): salty (solid), intermediate (dashed), fresh (dot-dashed), and no mixed-layer (dotted), and for Atlantic basin (gray). (c) zonal wind stress for base runs (no marker, smaller southern values), narrow single-basin perturbation experiments (circles), and all other perturbation experiments (no marker, larger southern values).

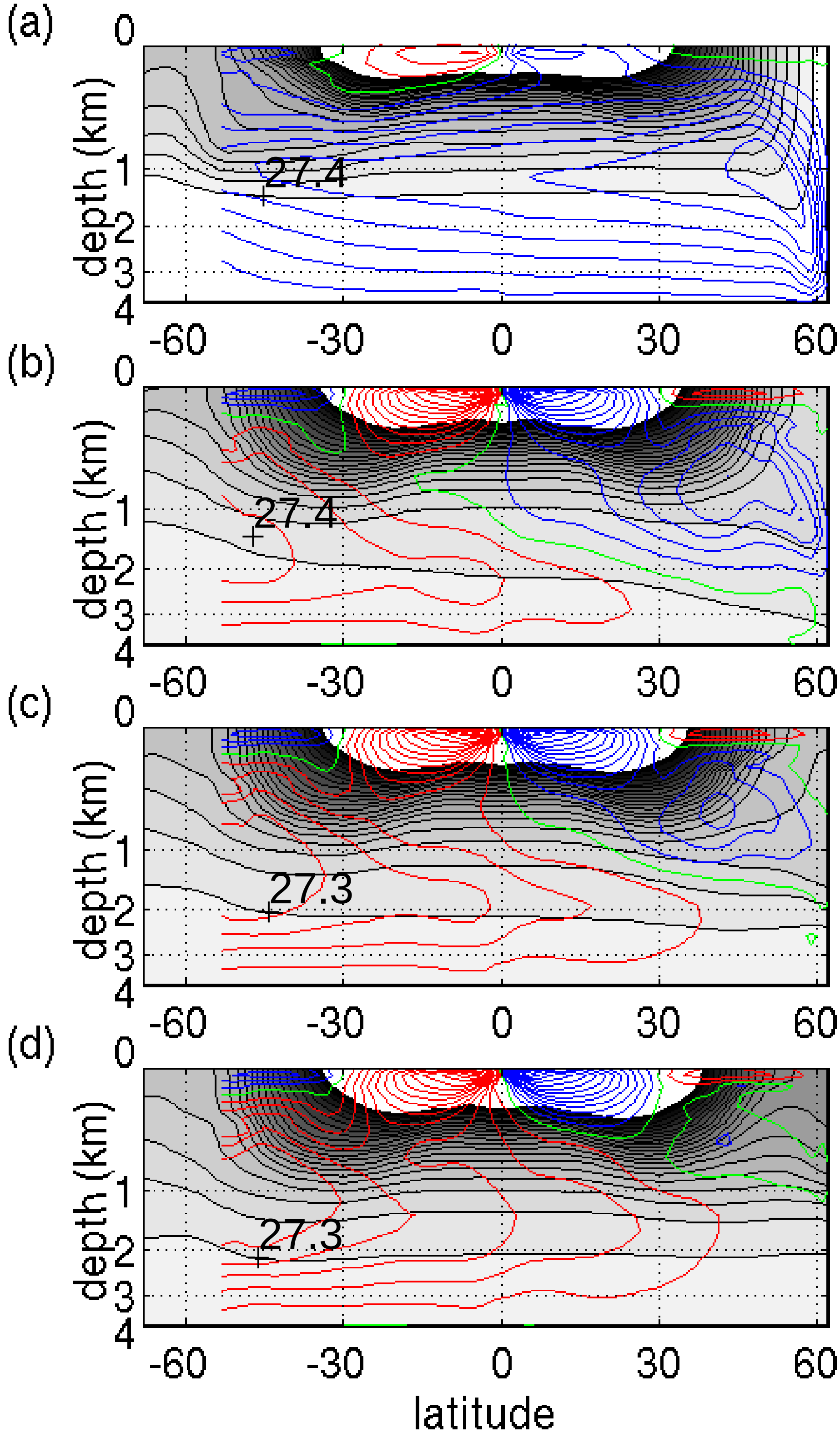

Figure 3: Base run zonal-average σ_θ (shading and black contours) and overturning (blue for northern-sinking, red for southern-sinking, green for zero contour) for (a) Atlantic basin of wide-light run, and Pacific basin for (b) wide-dense run, (c) wide-intermediate run, and (d) wide-light run. Contour interval is .1 kg/m^3 for σ_θ and 2 Sv for overturning.

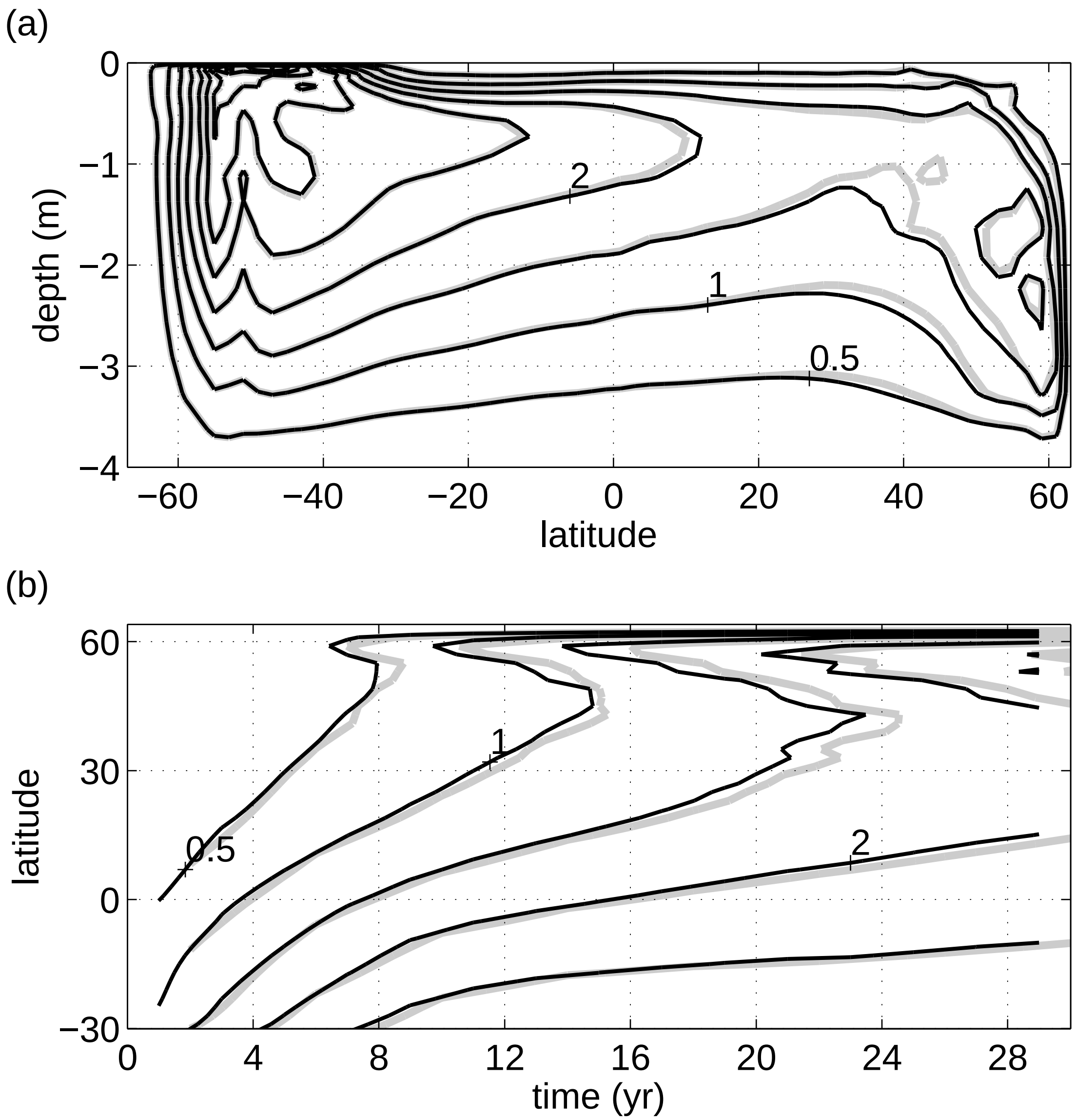

Figure 4: Comparison of overturning anomaly for equal timesteps (black) and long tracer timesteps (gray). (a) Streamfunction anomaly $\Phi'(\phi, z)$ averaged over 24 to 28 yr of model run. (b) Volume transport anomaly $\Phi'_M(t, \phi)$. For both panels, contour interval is .5 Sv.

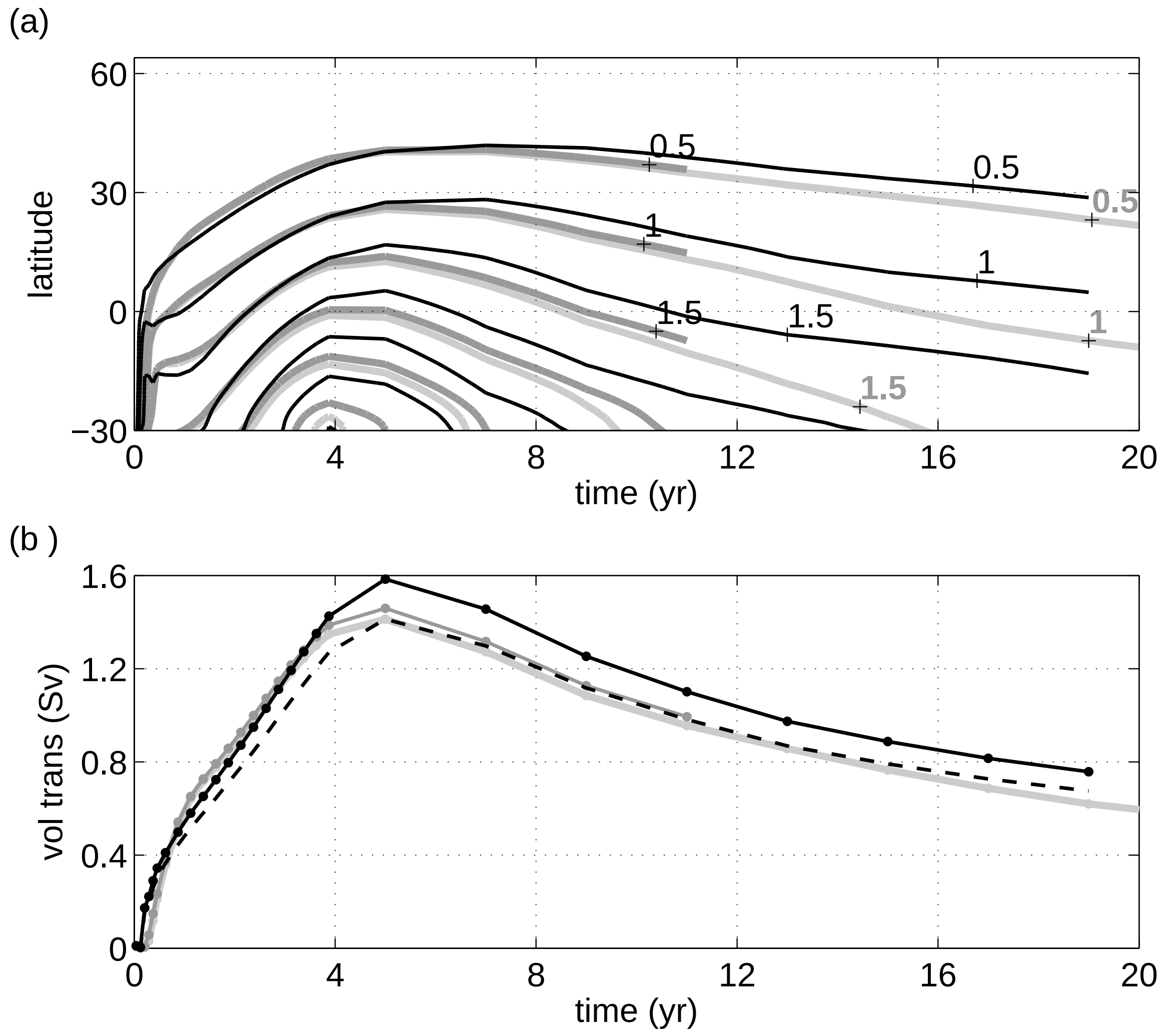

Figure 5: Comparison of overturning anomaly for perturbation from rest experiments with 2^o resolution (thick, light gray), 1^o (thick, dark gray), and 1^o low-ν_H (black), showing (a) $\Phi'_M(t, \phi)$ and (b) $\Phi'_M(t, 15^o\ N)$ (middle panel). In (a), contour interval is .5 Sv. In (b), dashed curve represents low-ν_H experiment scaled so that peak value is the same as the peak value of the 2^o experiment.

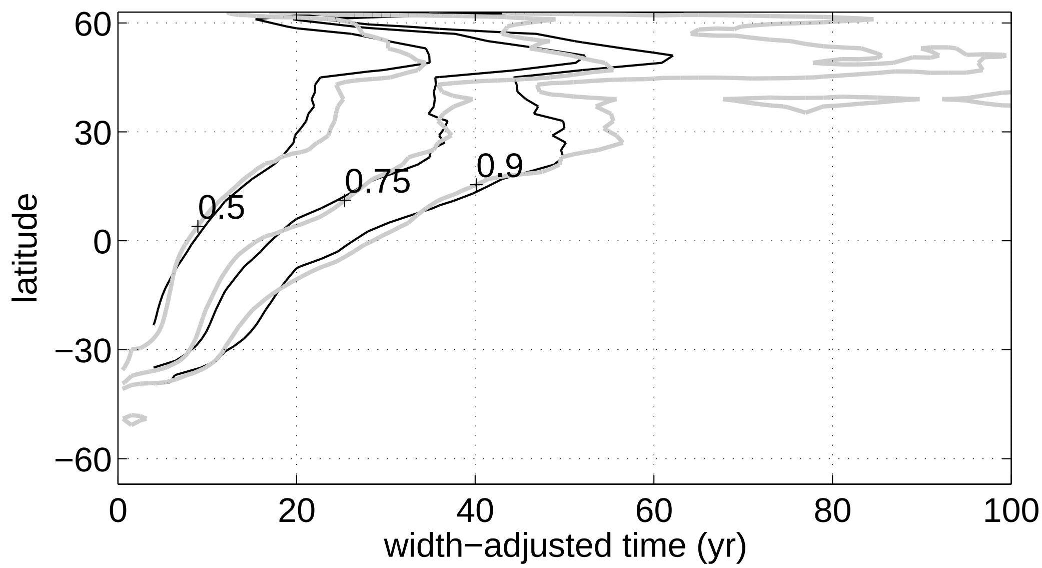

Figure 6: $\Phi_N(t_W, \phi)'$ (volume transport anomaly normalized by final values) for narrow (black) and wide (gray) single-basin experiments.

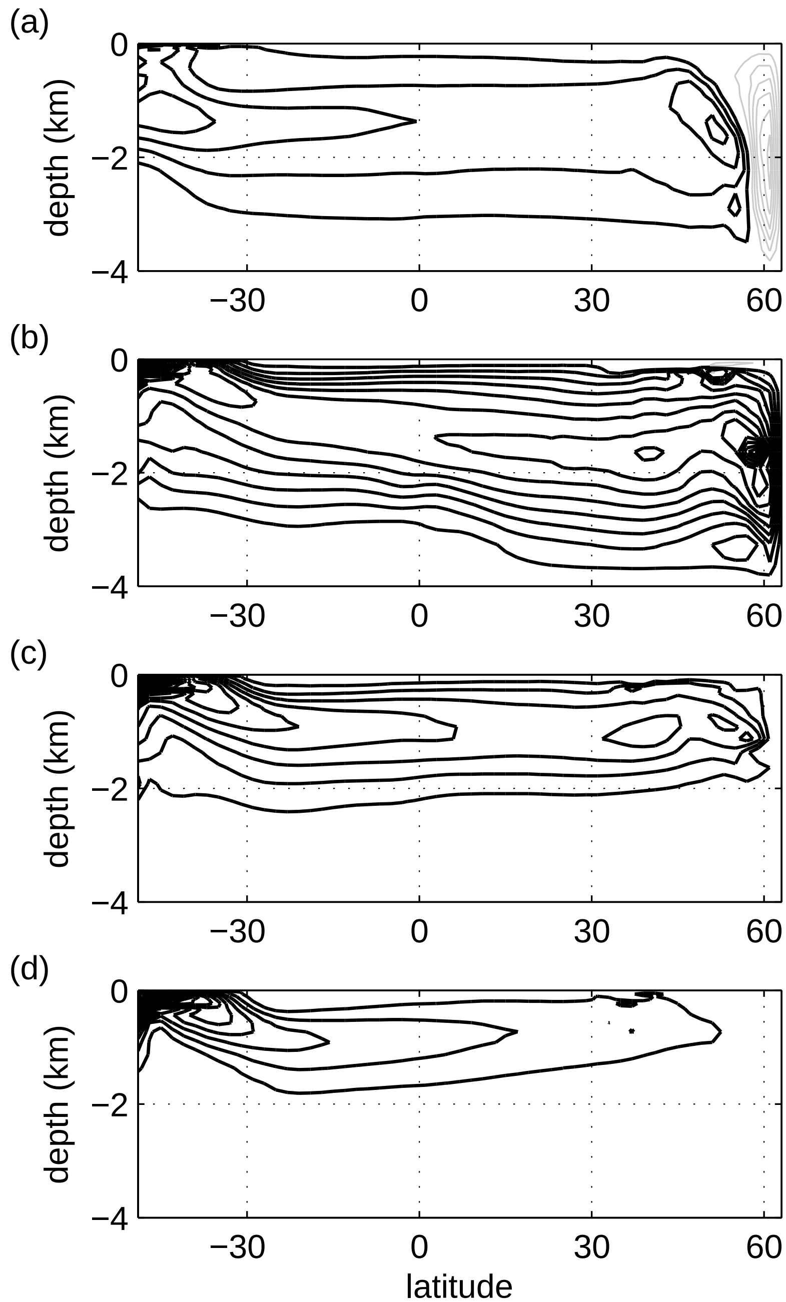

Figure 7: Final overturning anomaly Φ' corresponding to base run overturning shown in Fig. 3. (a) Atlantic basin of wide-light run, and Pacific basin for (b) wide-dense run, (c) wide-intermediate run, and (d) wide-light run. Contour interval is .5 Sv, northern-sinking shown in black, southern-sinking in gray.

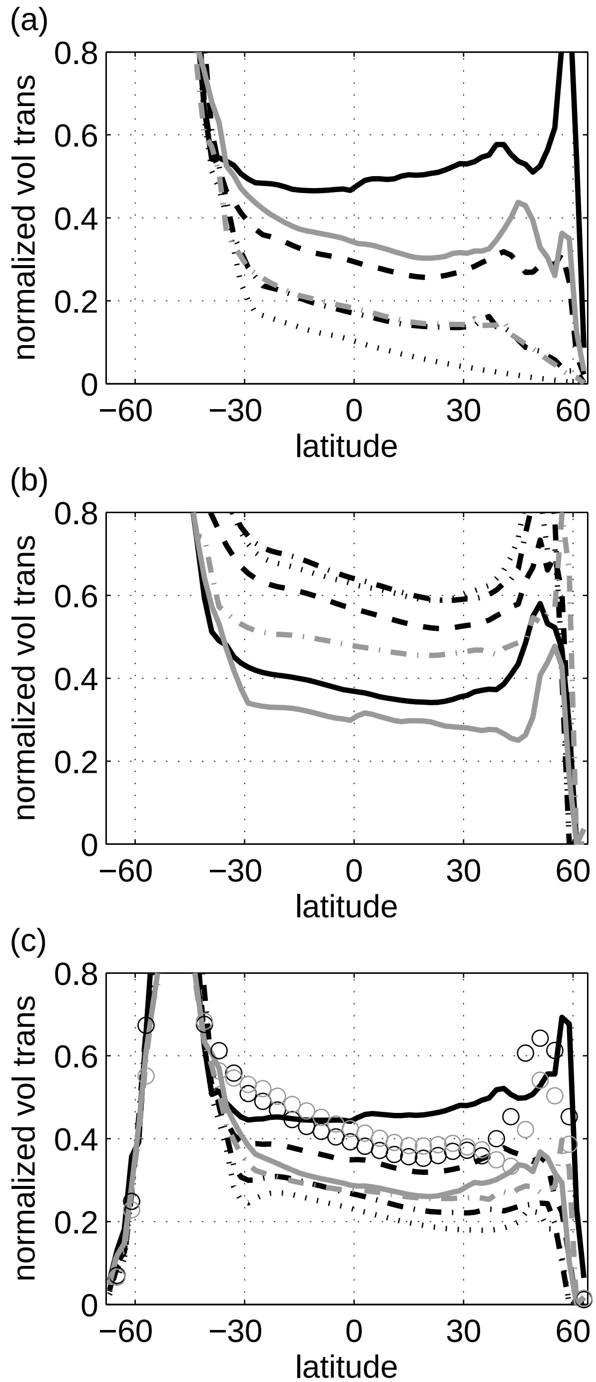

Figure 8: Final Φ'_M normalized by zonally-integrated Ekman transport in basin for $\Delta\Phi$ for (a) Pacific, (b), Atlantic, and (c) Globe. Experiment parameters include narrow (gray) and wide (black) Pacific, and dense (solid), intermediate (dashed), light (dash-dotted), and no-mixed-layer (dotted) Pacific. Single-basin experiments (circles) are shown in (c) only.

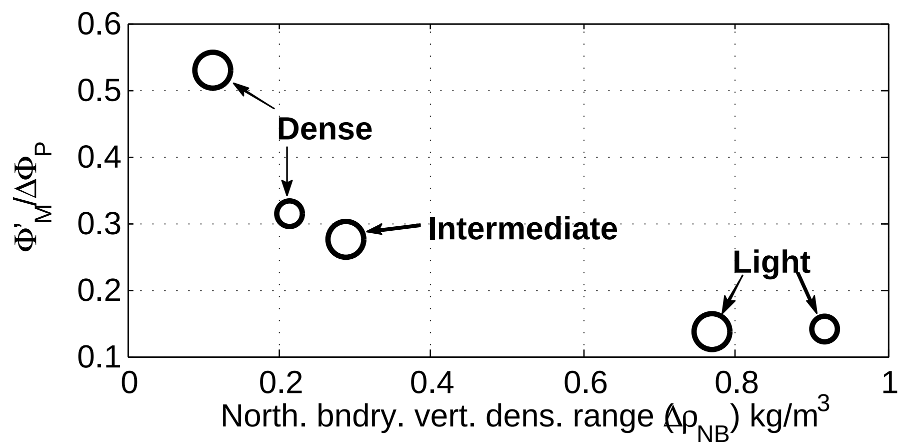

Figure 9: Pacific volume transport anomaly normalized by Pacific Ekman transport anomaly as a function of base run northern boundary vertical range of zonally averaged density (σ_θ) for wide-Pacific experiments.

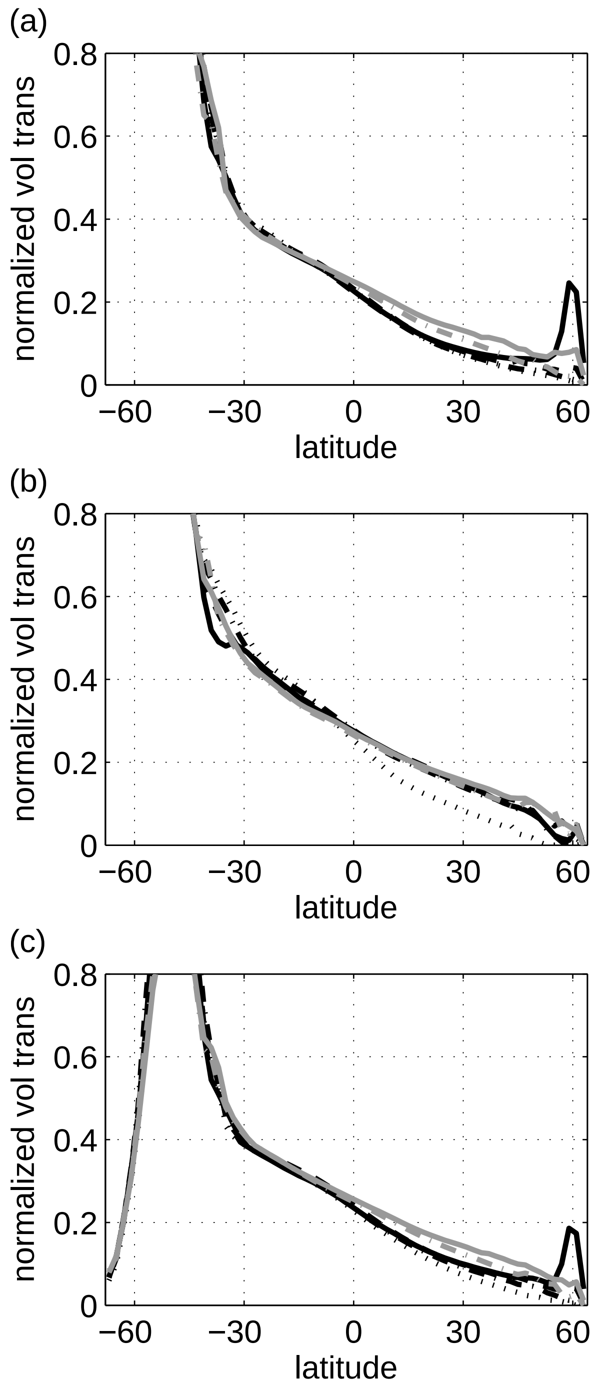

Figure 10: Like Fig. 8 for average from 8 to 10 yr. Note that not all experiments are visible because of overlap between different curves.

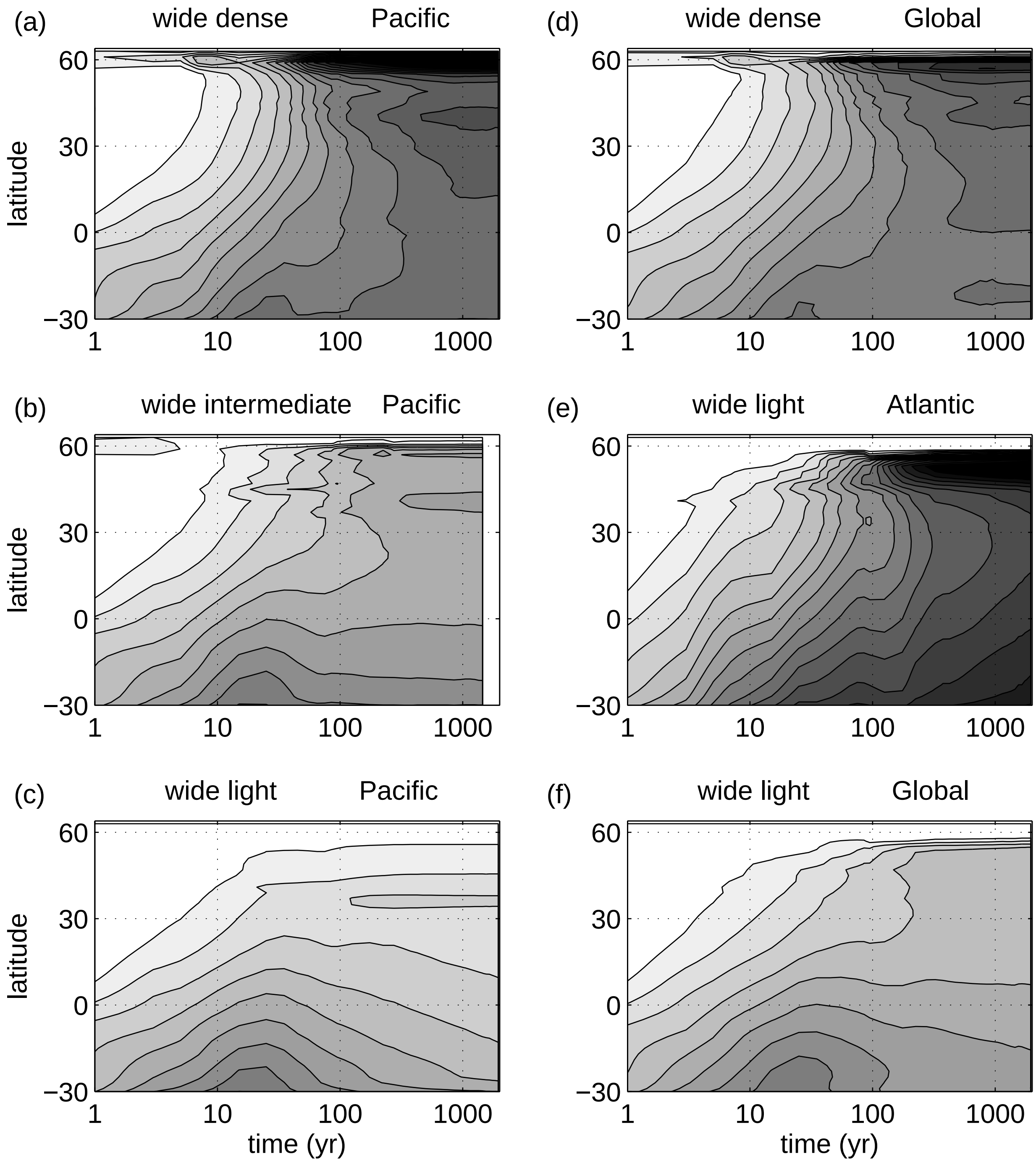

Figure 11: Φ'_M normalized by Ekman transport $\Delta\Phi$ as a function of time and latitude in Pacific (left panels), Atlantic (middle right panel), and entire domain (upper and lower right panels) for wide-dense run (top panels), wide-light run (bottom and middle-right panels), and wide-intermediate run (left middle panel). Contour interval is .05, with darker shading representing higher values.

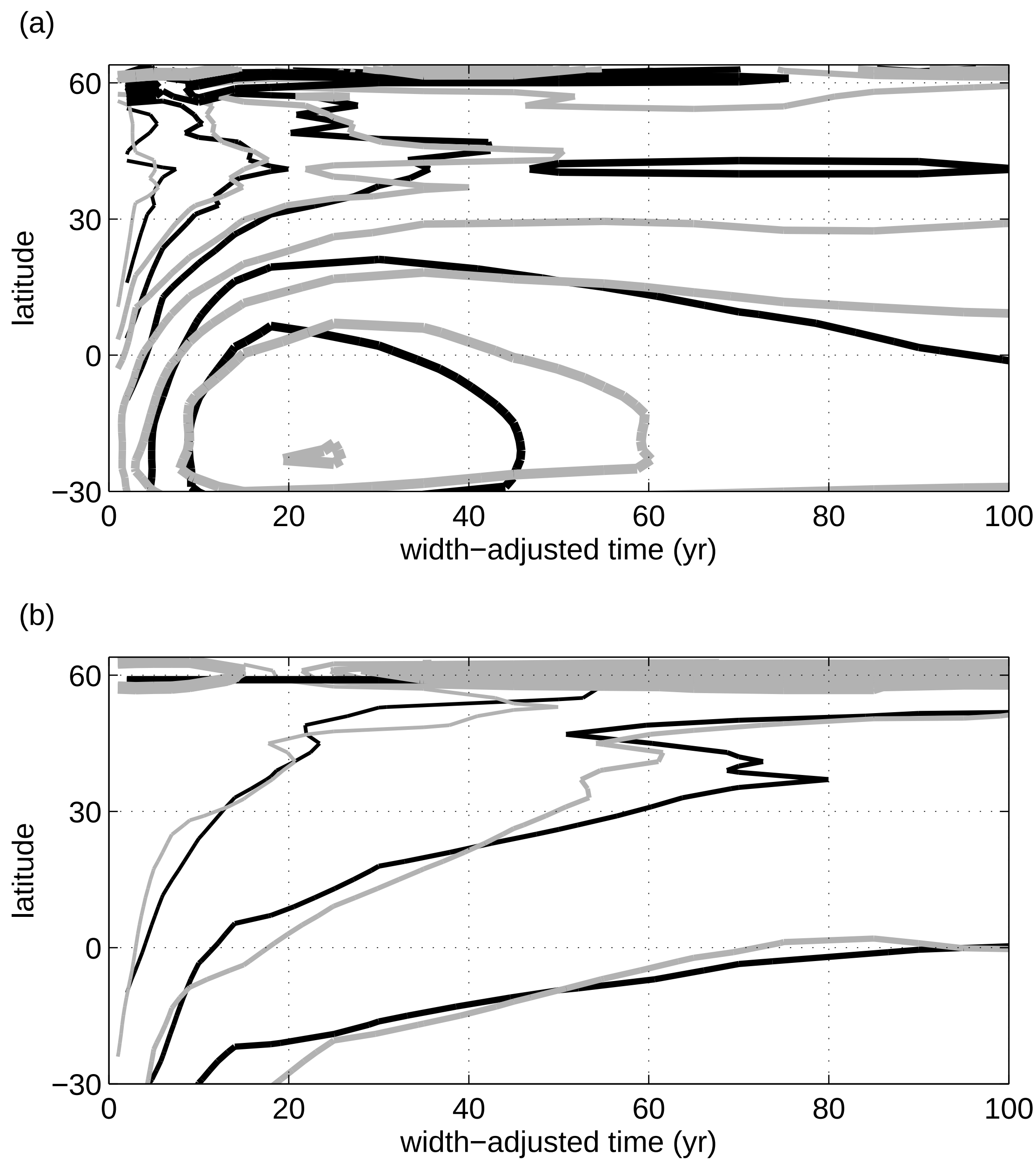

Figure 12: Normalized volume transport anomaly Φ'_N for (a) Pacific and (b) Atlantic as function of latitude and width-adjusted time for light narrow-Pacific experiment (black) and light wide-Pacific experiment (gray). Width adjusted time (see (2)) is calculated based on total domain width Λ and wide-Pacific domain width Λ_W. Contours for increasing values are shown with increasingly thick curves, starting at .25 with a contour interval of .25.

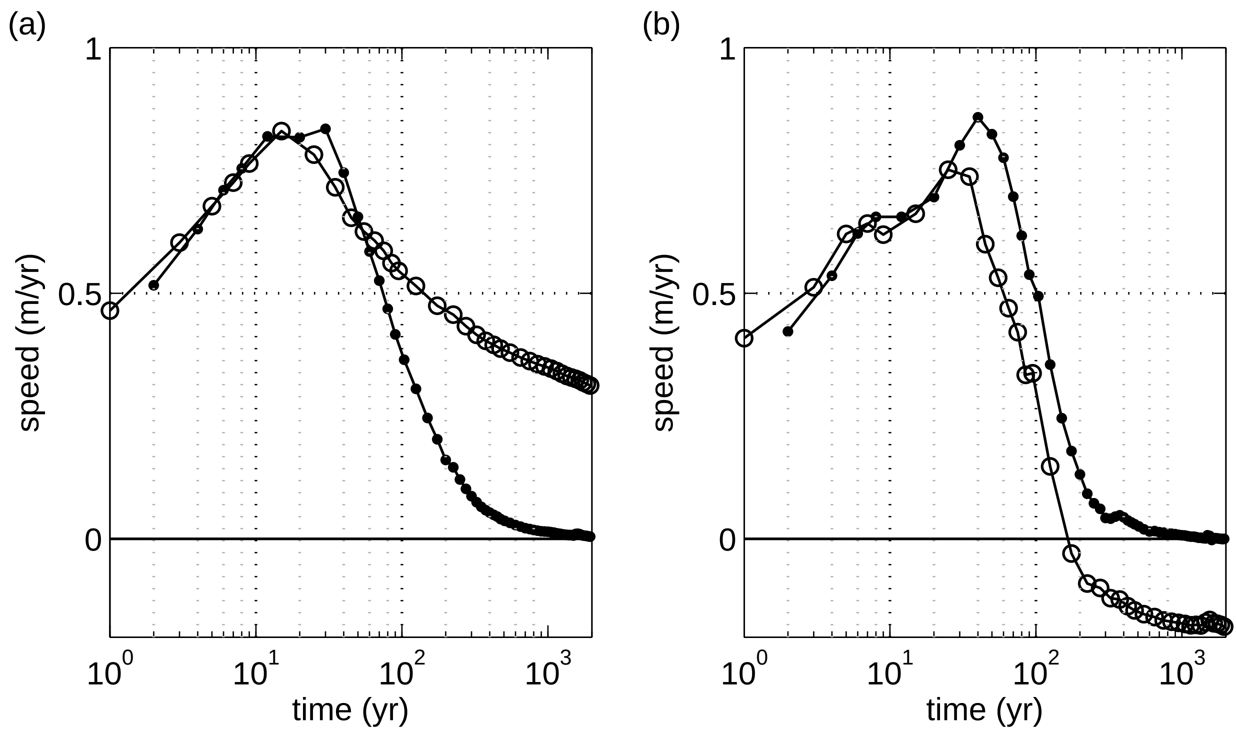

Figure 13: Vertical velocity anomaly of water parcels w (open circles) and isopycnal w_I (dots) at approximately 1000 m depth for (a) Pacific and (b) Atlantic of wide light-Pacific experiment.

Width	Initial State	Timestep	Resolution	ν_H (m^2/s)
80^o	forced	Bryan	2 deg	250×10^3
40^o	forced	Bryan	2 deg	250×10^3
40^o	forced	equal	2 deg	250×10^3
40^o	rest	equal	2 deg	250×10^3
40^o	rest	equal	1 deg	250×10^3
40^o	rest	equal	1 deg	10×10^3

Table 1. Summary of single-basin perturbation experiments. In "Initial State" column, "forced" refers to experiments integrated to near-equilibrium with parameters described in Section 2, and "rest" refers to horizontally-uniform initial state described in Section 2.

Pacific Density	Pacific Width
dense	40^o
dense	120^o
intermediate	120^o
light	40^o
light	120^o
no-mixed-layer	120^o

Table 2. Summary of double-basin perturbation experiments, with names in "Pacific Density" column referring to restoring profiles shown in Figure 2.